Reaction cross sections for proton scattering from stable and unstable nuclei based on a microscopic approach

H. F. Arellano[1,2,*] and M. Girod[2]

[1]*Department of Physics-FCFM, University of Chile, Av. Blanco Encalada 2008, Santiago, Chile*
[2]*Commisariat à l'Energie Atomique, Département de Physique Théorique et Appliquée, Service de Physique Nucléaire,
Boite Postale 12, F-91680 Bruyères-le-Châtel, France*

Reaction cross sections for proton-nucleus elastic scattering are investigated within a nonrelativistic microscopic approach for the nucleon-nucleus optical model potential. Applications were made for nucleon energy ranging between 10 MeV and 1 GeV, considering both stable and unstable target nuclei. The study is based on an *in-medium g*-matrix folding optical model approach in momentum space, with the appropriate relativistic kinematic corrections needed for the higher energy applications. The effective interactions are based on realistic NN potentials supplemented with a separable non-Hermitian term to allow optimum agreement with current NN phase-shift analyses, particularly the inelasticities above pion production threshold. The target ground-state densities are obtained from Hartree-Fock-Bogoliubov calculations based on the finite range, density-dependent Gogny force. The evaluated reaction cross sections for proton scattering are compared with measurements and their systematics is analyzed. A simple function of the total cross sections in terms of the atomic mass number is observed at high energies. At low energies, however, discrepancies with the available data are observed, being more pronounced in the lighter systems.

I. INTRODUCTION

Nucleon-nucleus integrated cross sections constitute a key observable in fundamental nuclear research as well as in applications of nucleon-induced reactions. These quantities are of particular importance in nuclear technology such as nuclear transmutation, nuclear waste treatment, safety assessment, and medical therapy. From a fundamental point of view, their description within global microscopic approaches constitutes a stringent test to the understanding of the underlying physics involved in the interaction of nucleons colliding with a nucleus. Depending on the energy range of the projectile, total cross sections may constitute an important input in the study of diverse phenomena. For instance, the study of *r* processes in astrophysics requires the knowledge of total cross sections at energies near and below a few MeV, whereas spallation applications may well require data up to GeV energies.

In this article we present a study of the systematics exhibited by proton-nucleus (*pA*) reaction cross sections based on the microscopic folding optical model potential approach of Arellano, Brieva, and Love [1,2], hereafter referred as ABL folding. The study spans in energy from a few MeV up to 1 GeV, considering various even-even isotopes from carbon up to lead. The calculated reaction cross sections are compared with existing data, whereas results for proton scattering from unstable nuclei are examined as functions of the number of constituents of the target.

Research on proton reaction cross sections of *pA* elastic scattering has received significant attention during recent years. These studies include experimental [3], phenomenolog-
ical [4,5], and microscopic [6–9] analyses. Global analyses in the framework of Glauber theory have also been reported [10]. Recent experimental efforts by Auce and collaborators [3] have been very valuable in reporting new measurements at intermediate proton energies. The phenomenological studies of Refs. [4] and [5] represent attempts to provide simple parametrizations of the observed cross sections in terms of geometry and mass distribution of the targets. The microscopic studies reported in Refs. [6–8] are based on the general *g*-folding framework reviewed in Ref. [11], where a medium-dependent NN effective interaction was folded with the target ground-state mixed density. In those studies a nonlocal optical potential is realized with the use of an antisymmetrized effective interaction of the form $g(\kappa', \kappa) = g_D(q) + g_{Ex}(Q)$, with $q = \kappa - \kappa'$, $Q = (\kappa + \kappa')/2$. The term $g_{Ex}(Q)$ leads to the nonlocality in the optical potential. The results reported in this work differ from those in Refs. [6–8] in two respects. First, the off-shell momentum space dependence of the antisymmetrized NN effective interaction, determined from complex NN bare potentials within the Brueckner-Bethe-Goldstone model, is retained without projection onto specific models as above. The second difference lies in the representation on the mixed density. Whereas the *g*-folding approach treats explicitly the mixed density extracted from shell models, the results reported here rely on its Slater representation requiring only the radial density. An assessment of this approximation has been made within the free *t*-matrix full-folding approach, where it is shown that it affects only slightly the differential scattering observables at momentum transfers below ∼1 fm⁻¹, becoming more visible above ∼2.5 fm⁻¹ (cf. Fig. 3 of Ref. [12]).

This article is organized as follows. In Sec. II we outline the general framework upon which we base our study. In Sec. III we present results for the calculated reaction cross sections for *pA* elastic scattering at energies between 10 MeV and 1 GeV.

---

*arellano@dfi.uchile.cl; http://www.omp-online.cl

Additionally, we examine the systematics exhibited by the calculated reaction cross sections and the total cross sections for neutron-nucleus (nA) elastic scattering at energies above 400 MeV. Finally, in Sec. IV we present a summary and the main conclusions of this work.

II. FRAMEWORK

In the nonrelativistic theory of the optical model potential for nucleon-nucleus scattering, the interaction between the projectile and the target is given by the double convolution of an NN antisymmetrized effective interaction with the target ground-state mixed density. In the ABL approach, the use of the Slater representation of the mixed density and the assumption of a weak dependence of the g matrix on one of the momentum integrals yield an optical potential for pA scattering of the form [1]

$$U_{pp}(\mathbf{k}', \mathbf{k}; E) = \int d\mathbf{Z} e^{i(\mathbf{k}'-\mathbf{k})\cdot\mathbf{Z}} \sum_{\alpha=p,n} \rho_\alpha(\mathbf{Z})\bar{g}_{p\alpha}[\mathbf{k}', \mathbf{k}; \rho_A(\mathbf{Z})],$$

(1)

where E is the pA center-of-mass energy, ρ_α is the point density of species α, and $\bar{g}_{p\alpha}$ represents an off-shell Fermi-averaged amplitude in the appropriate $p\alpha$ pair and evaluated at the local target density $\rho_A(\mathbf{Z})$. More explicitly, in an infinite nuclear matter model these density-dependent amplitudes are given by

$$\bar{g}_{NN}(\mathbf{k}', \mathbf{k}; \bar{\rho}) = \frac{3}{4\pi\hat{k}^3} \int \Theta(\hat{k} - |\mathbf{P}|)g(\mathbf{k}_r', \mathbf{k}_r; \sqrt{s}; \bar{\rho})d\mathbf{P},$$

(2)

where $g(\mathbf{k}_r', \mathbf{k}_r; \sqrt{s}; \bar{\rho})$ corresponds to off-shell g-matrix elements for symmetric nuclear matter of density $\bar{\rho}$. The relative momenta $\mathbf{k}_r'$ and $\mathbf{k}_r$ depend on the asymptotic momenta $\mathbf{k}'$ and $\mathbf{k}$, as well as on $\mathbf{P}$, the mean momentum of the struck target nucleon. Their general form is $\mathbf{k}_r = W\mathbf{k} - (1 - W)\mathbf{p}$, with $\mathbf{p} = \mathbf{P}/2 + \mathbf{k} - \mathbf{k}'$, and $W = W(E; \mathbf{k}', \mathbf{k}, \mathbf{P})$. As there is no local prescription to handle the g matrix, the results we report here retain the intrinsic nonlocalities of the NN interaction. The s invariant specifies the energy at which the interaction is evaluated, which depends on the energy E and the kinematics of the interacting pair. Details about the implementation of the Fermi-averaged elements and relativistic kinematics corrections are discussed in Ref. [2]. With the above considerations we obtain a nonlocal optical potential that is handled exactly within numerical accuracy.

An important element for the realization of the optical potential is the two-body effective interaction, which in our model takes the form of the nuclear matter g matrix. This is based on the Brueckner-Bethe-Goldstone model for symmetric nuclear matter described by the integral equation

$$g(\omega) = V + V\frac{\hat{Q}}{\omega - \hat{e}_1 - \hat{e}_2}g(\omega),$$

(3)

with V the free-space two-nucleon potential, $\hat{e}_1$ and $\hat{e}_2$ the quasiparticle energies, $\hat{Q}$ the Pauli blocking operator, and ω the starting energy just above the real axis. In the case of the

free t-matrix applications, the Pauli blocking operator is set to unity and the nuclear self-consistent fields vanish. Thus, $g \to t$, the NN scattering matrix in free space.

A physically acceptable g matrix for GeV-energy applications requires a bare NN potential model consistent with its high energy phenomenology, particularly the presence of complex phase-shifts above pion-production threshold [13]. In our approach this is achieved by supplementing realistic NN potential models (V_R) with a separable term of the form [2]

$$V = V_R + |\xi\rangle\Gamma(E)\langle\xi|.$$

(4)

In this study the form factors $|\xi\rangle$ are taken as harmonic oscillator states characterized with $\hbar\omega = 450$ MeV. The strength $\Gamma(E)$ is energy and state dependent, becoming complex in those states where loss of flux is observed. These coefficients are calculated analytically for each state to reproduce the year 2000 np continuous-energy solution (SP00) of the phase-shift analysis by Arndt *et al.* [13]. With these considerations we are able to account for the absorption stemming from the elementary NN interactions. Because most realistic bare potentials do not share a common phase-shift data basis, in particular the SP00 solution, we suppress the separable contribution below 300 MeV. The inclusion of the separable strength is done gradually out to 400 MeV, energy from which the full strength is taken into account.

Another important input in our calculations is the target ground-state radial density. This is obtained following self-consistent Hartree-Fock-Bogoliubov calculations with the Gogny force [14,15]. This interaction contains a central finite-range term, a zero-range spin-orbit contribution and a zero-range density-dependent contribution. This approach has been instrumental for obtaining the spherical radial densities for ^{12}C and the isotope families $^{12-26}$O, $^{34-64}$Ca, $^{50-86}$Ni, $^{80-100}$Zr, $^{96-136}$Sn, and $^{176-224}$Pb included in this study.

III. APPLICATIONS

A. Scattering from stable nuclei

Following the considerations outlined above, we have calculated the reaction cross sections (σ_R) for proton-nucleus elastic scattering at beam energies ranging from 5 MeV up to 1 GeV. The targets considered are ^{208}Pb, ^{90}Zr, ^{60}Ni, ^{58}Ni, ^{40}Ca, ^{16}O, and ^{12}C, whose proton and neutron root-mean-square (r.m.s.) radii are summarized in Table I. The results for σ_R are shown in semi-log scale in Fig. 1, where the data are taken from Ref. [3] (open squares), Ref. [16] (solid circles), and Ref. [17] (triangles). The calcium and nickel data are colored blue and red, respectively, to distinguish them when they overlap. The solid curves represent results from the ABL optical model using the nuclear matter g matrix based

TABLE I. Root-mean-square radii of the point proton (R_p) and neutron (R_n) densities used in this study.

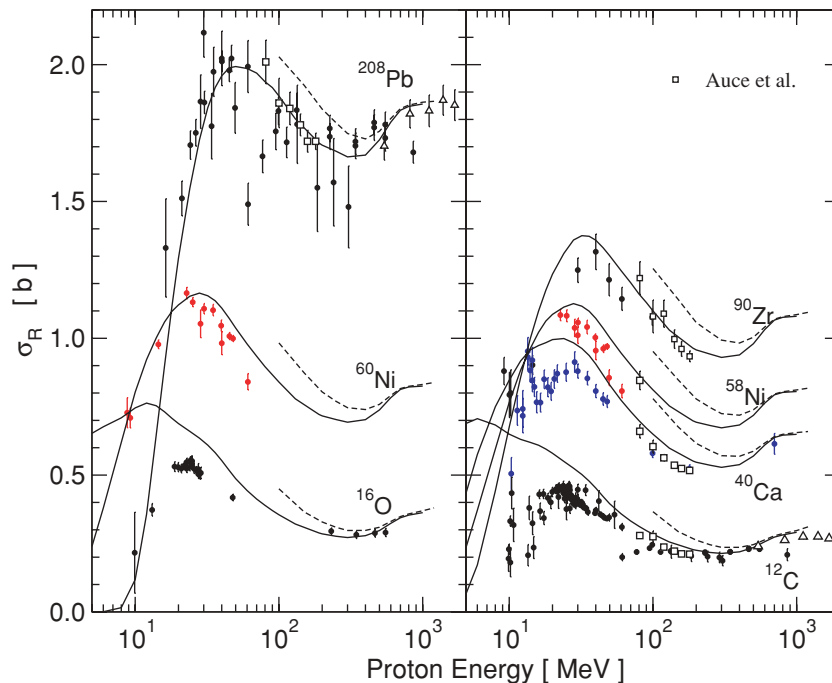| Nucleus	^{208}Pb	^{90}Zr	^{60}Ni	^{58}Ni	^{40}Ca	^{16}O	^{12}C
R_p [fm]	5.437	4.210	3.717	3.695	3.405	2.676	2.419
R_n [fm]	5.573	4.265	3.738	3.683	3.365	2.656	2.402

FIG. 1. (Color online) Measured [3,16,17] and calculated reaction cross sections based on ABL approach using the g matrix (solid curves) and the free t matrix (dashed curves).

on the np Argonne V18 reference potential [18], whereas the dashed curves represent results using the free t matrix corresponding to the same potential. As observed, the level of agreement between the calculated cross sections and the data is qualitatively different above 200 MeV from that below 100 MeV. At proton energies below 100 MeV, with the exception of ^{208}Pb, all results overestimate σ_R, being more pronounced for the ^{12}C and ^{16}O targets. In these two cases differences of $\sim$100 mb at 30 MeV are observed, with no proper account of the maxima near 25 MeV exhibited by the data. Instead, the calculated cross sections decrease monotonically in the range 10–300 MeV. This feature is also observed in Ref. [9], where a much closer agreement between the calculations and the data is reported. The deficiencies of microscopic optical models at low energies have been addressed recently in Ref. [19], where it is suggested that the inclusion of nucleon-phonon couplings may be needed to improve the agreement with the low energy data.

For the heavier targets (^{40}Ca, ^{58,60}Ni, ^{90}Zr, and ^{208}Pb), the calculated cross sections follow the same qualitative trend of the data. The discrepancies observed at energies between 20 and 100 MeV can be characterized by a uniform 50 mb overestimate of the calculated cross sections relative to the data. At energies above 200 MeV the agreement with the measured cross sections is considerably improved, with the exception of the 860 MeV measurements of ^{12}C and ^{208}Pb, where a clear disagreement is observed. At this particular energy we have performed optical model calculations for the targets considered and our predictions are summarized in Table II. These predictions are consistent with the data from Ref. [17] near and above 1 GeV (open triangles), an indication of the adequacy of our approach at these high energies.

For completeness in this section, in Fig. 2 we compare the measured [20] and calculated nA total cross sections (σ_T). The calculated results are based on the ABL folding

approach covering the energy range between 5 MeV and 1 GeV. What becomes clear from this figure is that the closest agreement with the data occurs for the lighter self-conjugate targets; instead, the calculated σ_T for the isospin asymmetric systems ^{90}Zr and ^{208}Pb lack the pronounced oscillating pattern exhibited by the data bellow 200 MeV. Microscopic calculations within the g-folding approach have been reported [9] to provide an excellent account for the total cross section data in the 60–200 MeV energy range. Its extension to 600 MeV has been achieved by means of a simple parametric form [21]. From the perspective of the microscopic ABL approach, the proper account for σ_R in the case of isospin asymmetric targets remains an open issue.

B. Scattering from unstable isotopes

To explore the behavior of the integrated cross sections as functions of the mass number, particularly its isotopic asymmetry, we evaluated σ_R and σ_T for nucleon-nucleus elastic scattering. These applications include results at 0.4, 0.7, and 1.0 GeV nucleon energies, covering the even-even

TABLE II. Measured [16] and predicted σ_R for pA scattering at 860 MeV.

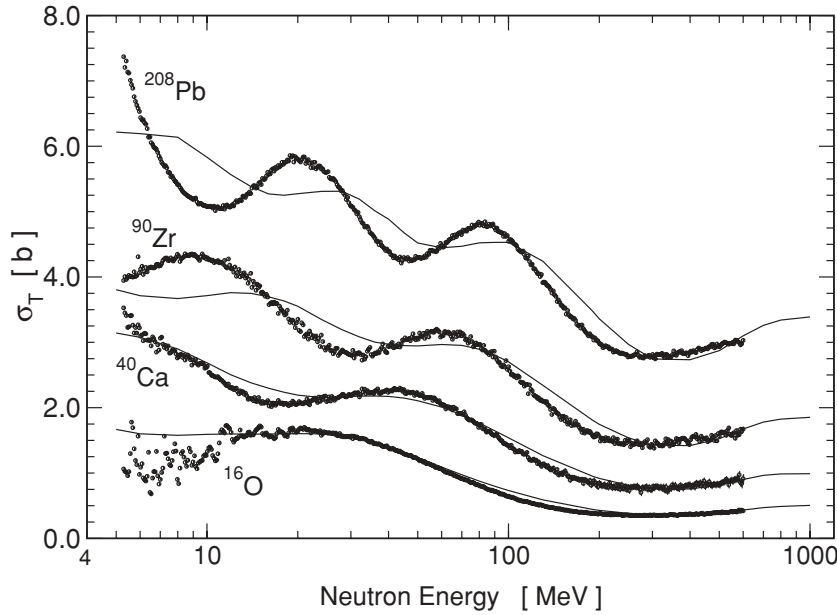| Target	Measured σ_R [mb]	Predicted σ_R [mb]
^{208}Pb	1680±40	1852
^{90}Zr	–	1079
^{60}Ni	–	823
^{58}Ni	–	804
^{40}Ca	–	647
^{16}O	–	357
^{12}C	209±22	284

FIG. 2. The measured [20] and calculated total cross sections based on the in-medium ABL optical model approach.

isotopes of oxygen, calcium, nickel, zirconium, tin, and lead. In Fig. 3 we show a log-log plot of the calculated σ_R (red circles) and σ_T (blue circles) at 0.4, 0.7, and 1.0 GeV nucleon energy as functions of A, the number of nucleons of the target. The straight lines represent the least-square regression of the type

$$\sigma = \sigma_0 A^p, \tag{5}$$

with σ_0 the reduced cross section and p the power-law exponent. Both parameters depend on the nucleon energy E. For clarity in the figure, the results for 0.7 and 1.0 GeV have been offset by factors of 10 and 100, respectively.

As observed from the figure, with the exception of σ_R for the oxygen isotopes, the overall trend of the calculated cross

sections follows very well the A^p power law. In the case of the oxygen isotopes at 1.0 GeV, a slight deviation as a function of the asymmetry $A - 2Z$ is perceived. In this particular case the maximum deviation of the calculated σ_R with respect to the A^p law is bound by 3%. Our estimate is that this manifestation of the isotopic asymmetry is genuine, although a more reliable assessment would require a better handling of the target mixed density. Such considerations go beyond the scope of the present work.

In Table III we summarize the results from the power law regression of the calculated cross sections. In all cases we include the standard deviation of the obtained reduced cross section and corresponding exponent. Judging by the standard deviation, the results at 1 GeV exhibit the closest agreement with the A^p behavior, a case in which $\sigma_R \sim A^{0.644}$ and
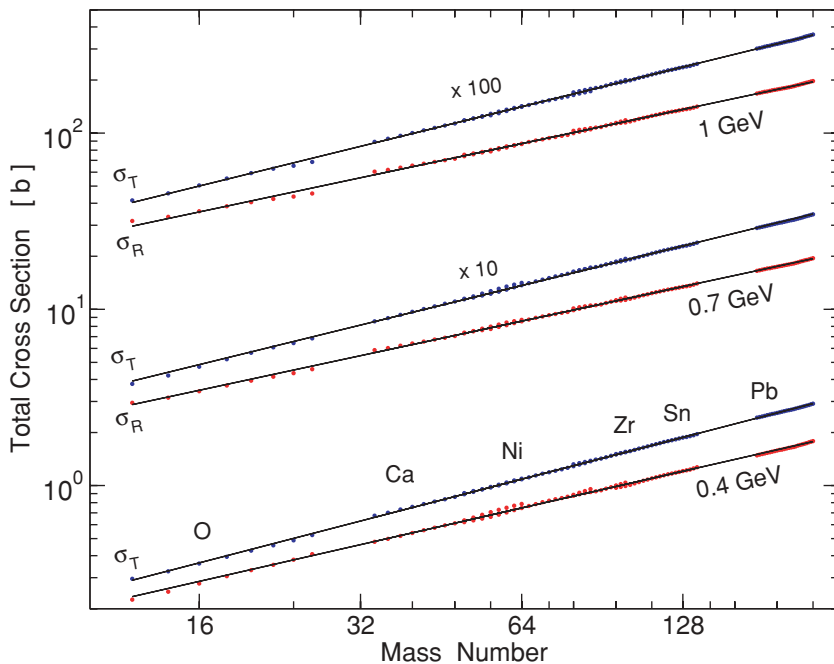

FIG. 3. (Color online) Calculated σ_R and σ_T for nucleon elastic scattering from O, Ca, Ni, Zr, Sn, and Pb even-even isotopes. The lower, middle, and upper pair curves correspond to 0.4, 0.7, and 1.0 GeV nucleon energy, respectively.

TABLE III. Results for the A^p power law regression of the calculated cross sections as a function of the nucleon energy.

E [GeV]	σ_R		σ_T	
	σ_0 [mb]	p	σ_0 [mb]	p
0.4	42.0±0.1	0.692±0.003	40.9±1.1	0.789±0.005
0.7	57.0±0.8	0.652±0.002	61.4±0.8	0.746±0.002
1.0	59.8±0.1	0.644±0.002	63.0±0.1	0.747±0.001

$\sigma_T \sim A^{0.748}$. Clearly these results differ from the $A^{2/3}$ geometric law, suggesting the relevance of the hadron dynamics and implicit correlations in the collision phenomena.

A closer comparison between the calculated cross section and the least-square power law fit is shown in Fig. 4, where the solid curves represent the cross sections for nucleon scattering from ^{16}O at 1 GeV using the corresponding parameters from Table III. The solid circles represent the calculated σ_R and σ_T using the ABL approach, where dashed lines are drawn to guide the eye. In this figure the departure from the A^p behavior when the neutron number varies becomes evident. Indeed, the calculated cross sections are weaker than those obtained from the power law for increasing neutron excess. Conversely, the oxygen isotopes with fewer neutrons than protons yield cross sections greater than the ones prescribed by the parametrization. These features become more pronounced in σ_R than in σ_T. Although we do not have a thorough explanation of this feature, we notice that the elementary total cross sections, σ_{pp} and σ_{pn}, grow very rapidly between 500 MeV and 1.3 GeV nucleon laboratory energy. This increase is more pronounced in σ_{pp} than in σ_{pn}, where σ_{pn} is overtaken by σ_{pp} near 1 GeV. The smaller σ_{pn} relative to σ_{pp} weakens the increase of the total cross section as the number of neutrons is increased.
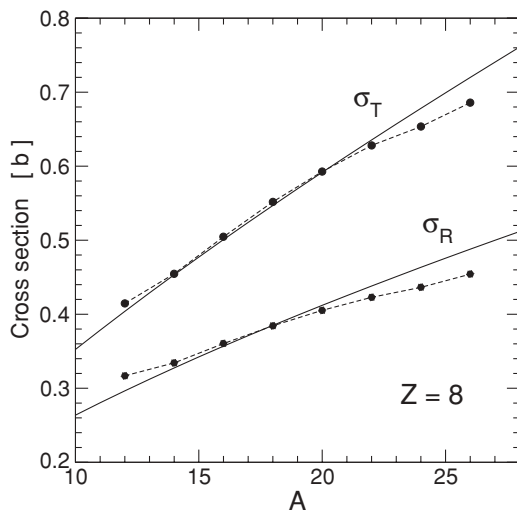

FIG. 4. The calculated σ_R and σ_T (solid circles) versus the A^p power law regression (solid curves) for 1 GeV nucleon scattering from oxygen isotopes.

IV. SUMMARY AND CONCLUSIONS

We have presented a global study of the reaction cross section for proton scattering from various stable and unstable isotopes at energies between 10 MeV and 1 GeV. The study is based on the microscopic in-medium ABL optical model potential approach, where the effective interaction is represented by the nuclear matter g matrix based on the Argonne AV18 NN potential. Inelasticities above the pion production threshold are accounted for by means of a non-Hermitian separable, energy-dependent term added to the NN reference potential. The separable contribution is adjusted to match the SP00 phase-shift analysis available from the George Washington University Data Analysis Center [13]. The target ground-state densities were obtained from Hartree-Fock-Bogoliubov calculations based on the finite range, density-dependent Gogny force.

We have found that the calculated reaction cross sections for pA scattering from stable nuclei are in reasonable agreement with the data above 200 MeV. This feature contrasts with the results for the lighter targets (^{12}C and ^{16}O) at energies below 100 MeV, where the ABL approach overestimates the data significantly. The situation for the total cross section for nA scattering is qualitatively the opposite, with a close agreement between the calculated and measured σ_T in the case of the self-conjugate targets and clear disagreement below 200 MeV for the isospin asymmetric (^{90}Zr and ^{208}Pb) targets. Thus far we have been unable to identify a microscopic mechanism able to account for these contrasting features.

We have also investigated the behavior of the calculated total cross sections as a function of the target mass number for various isotope families. We infer that both σ_R and σ_T follow an A^p power law accurate within 3% of the calculated values. At nucleon energies between 0.7 and 1.0 GeV the exponents for σ_R and σ_T are very close to 2/3 and 3/4, respectively. A slight deviation from this law is observed when the number of neutrons departs from that for the most stable isotope. This feature becomes more pronounced in the case of σ_R at 1 GeV for ^{16}O, but weakens for heavier targets and lower energies.

The work reported here constitutes a global assessment of the microscopic momentum-space ABL optical model approach on its account for proton reaction and neutron total cross section, covering nearly three orders of magnitude in energy. Similar studies have been reported within alternative theoretical approaches, such as Glauber theory [10], the in-medium g-folding approach, and global Dirac phenomenology [7]. Although some differences occur in the quality of the description of the data, particularly with respect to the g-folding approach, it remains difficult to identify the sources of such differences. Additionally, the representation of the mixed density may be critical in the case of light systems. In this regard, the g-folding approach is more detailed by making explicit use of the full mixed density based on shell models, a treatment which is pending in the ABL approach.

From a broader prospective, the realization of the ABL optical model relies on a weak dependence on the struck

nucleon momentum. This assumption is crucial to reduce the number of multidimensional integrals by three, making computationally feasible the evaluation of optical potentials [22]. However, the conditions under which this assumption becomes most (or least) adequate have not been investigated. Other aspects such as charge symmetry of the bare NN interaction and asymmetric nuclear matter effects may also need to be examined.

[1] H. F. Arellano, F. A. Brieva, and W. G. Love, Phys. Rev. C **52**, 301 (1995).

[2] H. F. Arellano and H. V. von Geramb, Phys. Rev. C **66**, 024602 (2002)

[3] A. Auce, A. Ingemarsson, R. Johansson, M. Lantz, G. Tibell, R. F. Carlson, M. J. Shachno, A. A. Cowley, G. C. Hillhouse, N. M. Jacobs, J. A. Stander, J. J. van Zyl, S. V. Förtsch, J. J. Lawrie, F. D. Smit, and G. F. Steyn, Phys. Rev. C **71**, 064606 (2005).

[4] A. Kohama, K. Iida, and K. Oyamatsu, Phys. Rev. C **72**, 024602 (2005).

[5] A. Ingemarsson and M. Lantz, Phys. Rev. C **72**, 064615 (2005).

[6] K. Amos, W. A. Richter, S. Karataglidis, and B. A. Brown, Phys. Rev. Lett. **96**, 032503 (2006).

[7] P. K. Deb, B. C. Clark, S. Hama, K. Amos, S. Karataglidis, and E. D. Cooper, Phys. Rev. C **72**, 014608 (2005).

[8] P. K. Deb and K. Amos, Phys. Rev. C **67**, 067602 (2003).

[9] P. K. Deb, K. Amos, S. Karataglidis, M. B. Chadwick, and D. G. Madland, Phys. Rev. Lett. **86**, 3248 (2001).

[10] A. de Vismes, P. Roussel-Chomaz, and F. Carstoiu, Phys. Rev. C **62**, 064612 (2000).

[11] K. Amos, P. J. Dortmans, H. V. von Geramb, S. Karataglidis, and J. Raynal, in *Advances in Nuclear Physics*, edited by J. W. Negele and Erich Vogt (Kluwer Academic/Plenum Publishers, New York, 2000), Vol. 25, p. 275.

[12] H. F. Arellano, F. A. Brieva, and W. G. Love, Phys. Rev. C **42**, 652 (1990).

[13] R. A. Arndt, I. I. Strakovsky, and R. L. Workman, Phys. Rev. C **62**, 034005 (2000). Also, CNS DAC (SAID), Physics Deptartment, The George Washington University, http://gwdac.phys.gwu.edu/.

[14] J. Dechargé and D. Gogny, Phys. Rev. C **21**, 1568-1593 (1980).

[15] J.-F. Berger, M. Girod, and G. Gogny, Comput. Phys. Commun. **63**, 365 (1991).

[16] R. F. Carlson, At. Data Nucl. Data Tables **63**, 93 (1996).

[17] F. S. Dietrich, E. P. Hartouni, S. C. Johnson, G. J. Schmid, R. Soltz, W. P. Abfalterer, R. C. Haight, L. S. Waters, A. L. Hanson, R. W. Finlay, and G. S. Blanpied, J. Nucl. Sci. Technol., Supplement **2**, 269 (2002).

[18] R. B. Wiringa, V. G. J. Stoks, and R. Schiavilla, Phys. Rev. C **51**, 38 (1995).

[19] M. Dupuis, S. Karataglidis, E. Bauge, J. P. Delaroche, and D. Gogny, Phys. Rev. C **73**, 014605 (2006).

[20] R. W. Finlay, W. P. Abfalterer, G. Fink, E. Montei, T. Adami, P. W. Lisowski, G. L. Morgan, and R. C. Haight, Phys. Rev. C **47**, 237 (1993).

[21] P. K. Deb, K. Amos, and S. Karataglidis, Phys. Rev. C **70**, 057601 (2004).

[22] H. F. Arellano and E. Bauge, Phys. Rev. C **76**, 014613 (2007).